

Internal vs. Fishhook Hairpin DNA: Different Unzipping Locations and Mechanisms in the α -Hemolysin Nanopore

Yun Ding, Aaron M. Fleming, Henry S. White, and Cynthia J. Burrows

Department of Chemistry, University of Utah, Salt Lake City, UT 84112-0850

Contents :

Single exponential decay fitting	SI3
Table SI 1. T_m analysis of internal hairpins	SI3
Figure S1. $i-t$ traces for I-hp12-1 at 100 mV with loop entry events.	SI4
Figure S2. $i-t$ traces for I-128hp12-1 at 100 mV.	SI5
Figure S3. $i-t$ traces for F-hp12-1 at 120 mV.	SI6
Figure S4. $i-t$ traces for dumbbell sequence at 100 mV.	SI7
Figure S5. Single exponential decay fitting of data for internal hairpins I-hp12-1, 2, 3, and 4 at 80 mV (A) and 100 mV (B)	SI8
Figure S6. Voltage dependence study of internal hairpins and fishhook hairpins.	SI9
Figure S7. Single exponential decay fitting of data for hp6, hp9, hp12, and hp15 at 80 mV (A) and 100 mV (B).	SI10
Figure S8. Single exponential decay fitting of data for fishhook F-hp12-1, 2, 3, and 4 at 80 mV (A) and 100 mV (B).	SI11
Figure S9. Urea denaturation study of internal hairpins.	SI12
Figure S10. The unzipping time distribution and the 2D plots for internal hairpin I-hp12-1 at 80 mV, 100mV, and 120mV.	SI13
Figure S11. The unzipping of two internal hairpins with different tail length at different voltages.	SI14
Figure S12. Unzipping Directionality of internal hairpins.	SI15
Figure S13. Sample $i-t$ traces of I-hp12-1 and F-hp12-1 unzipping in the same protein channel.	SI16
Figure S14. Single internal hairpins events shown in Figure S9.	SI17
Figure S15. Representative internal hairpin $i-t$ traces for the long asymmetric hairpin at 100 mV.	SI18

Figure S16. <i>i-t</i> traces for I-hp6 at 100 mV.	SI19
Figure S17. <i>i-t</i> traces for I-hp15 at 100 mV.	SI20
Figure S18. <i>i-t</i> traces for internal hairpin with asymmetric tails ($X = 6$) at 100 mV.	SI21
Figure S19. <i>i-t</i> traces for internal hairpin with asymmetric tails ($X = 9$) at 100 mV.	SI22
Figure S20. <i>i-t</i> traces for internal hairpin with asymmetric tails ($X = 12$) at 100 mV.	SI23
Figure S21. Blocking current of fishhook hairpin from 5' entry.	SI24

Single exponential decay fitting: The equation used in the single exponential decay fitting is:

$$y = A_1 * \exp(-x/\tau) + y_0$$

x is the duration in ms; y is the counts; τ is unzipping time in ms; A_1 is amplitude and y_0 is offset.

T_m Analysis: The hairpin samples were dissolved in buffer (10 mM PBS, pH 7.4, 1.00 M KCl) at a 1 μ M concentration, followed by heating the sample at 90 °C for 5 min. Then the samples were flash cooled by putting them into ice. Next, the samples were loaded into T_m analysis cuvettes following the manufacturer's protocol (SHIMADZU UV-1800) and placed into a UV/vis spectrophotometer. Samples were thermally equilibrated at 30 °C for 20 min followed by heating to 95 °C at a rate of 0.5 °C/min. As the samples were heated, absorbance readings at 260 nm and 280 nm were taken every 0.5 min. The background corrected data were plotted, and the T_m values were determined using first derivative analysis.

Table SI 1. T_m analysis of internal hairpins.

T_m /°C	I-hp12-1	I-hp12-2	I-hp12-3	I-hp12-4
	83.5±0.5	86.5±0.8	86.4±0.6	82.3±1.0

Figure S1. Internal hairpin *i-t* traces for I-hp12-1 at 100 mV (*trans* vs. *cis*) with loop entry events. Loop entry events are circled.

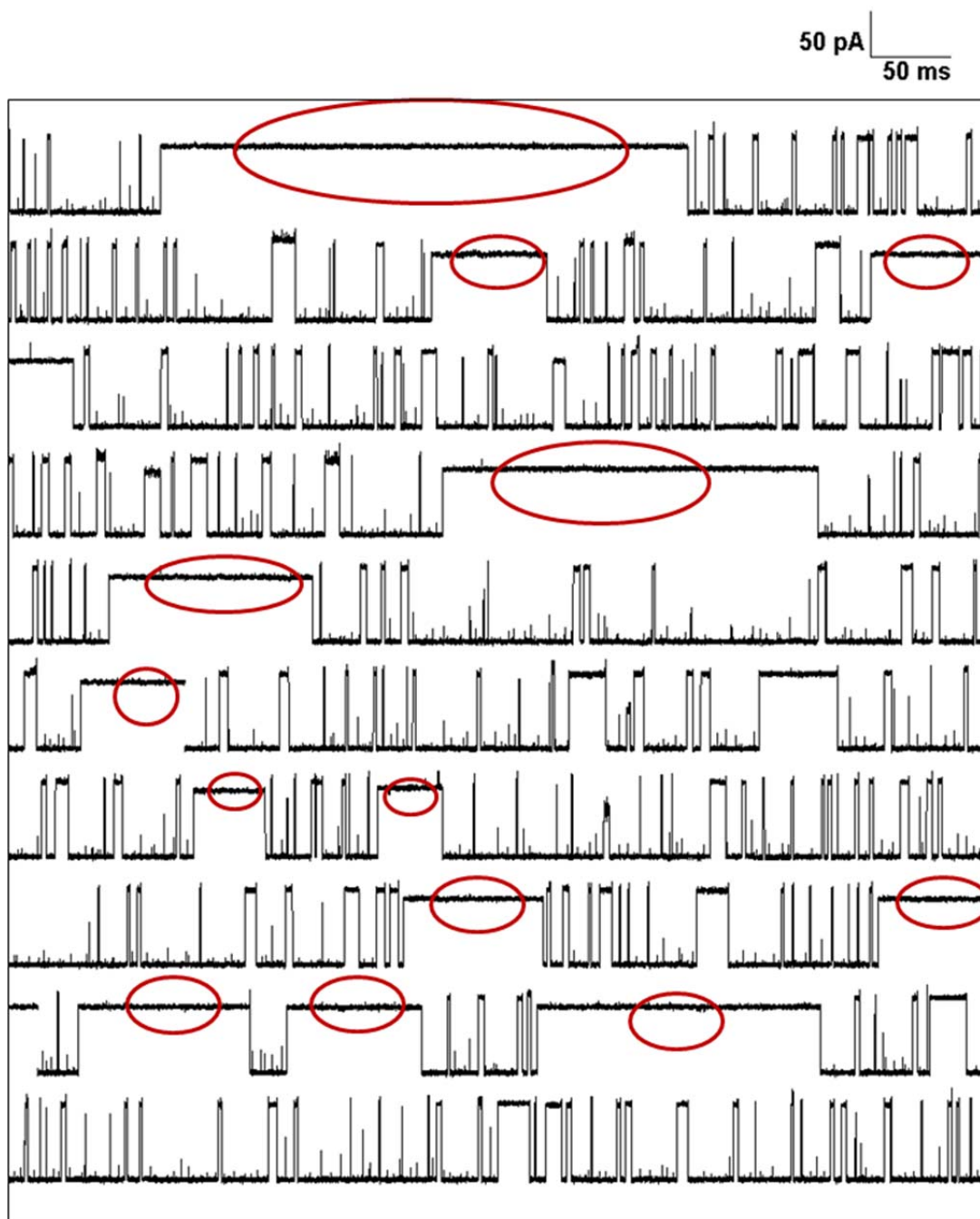


Figure S2. Internal hairpin *i-t* traces for I-128hp12-1 at 100 mV (*trans* vs. *cis*). Loop entry events were longer than ~200 ms and less blocking than those of fast, deep-blocking translocation events.

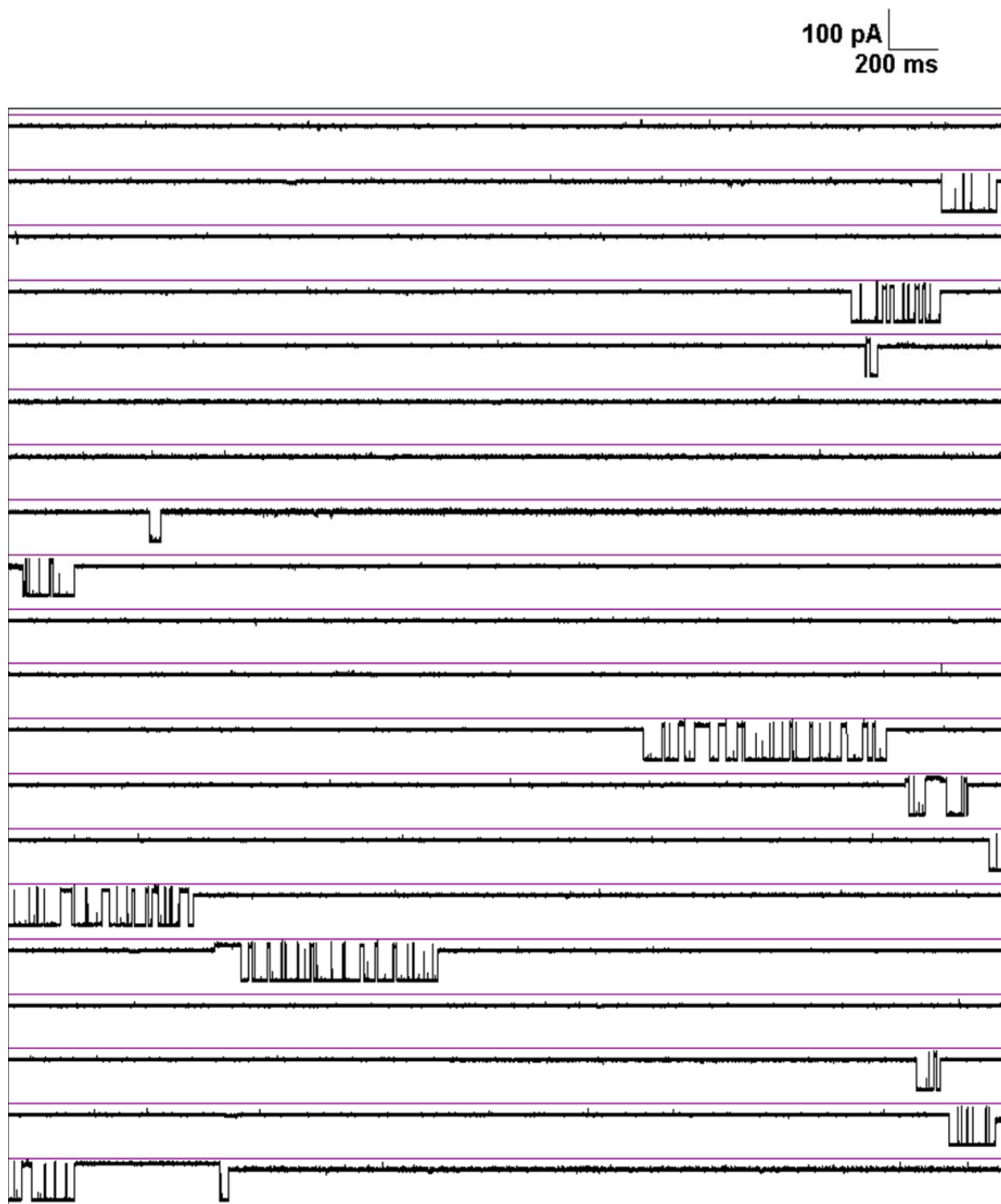


Figure S3. Fishhook hairpin *i-t* traces for F-hp12-1 at 120 mV (*trans* vs. *cis*). Loop entry events are circled.

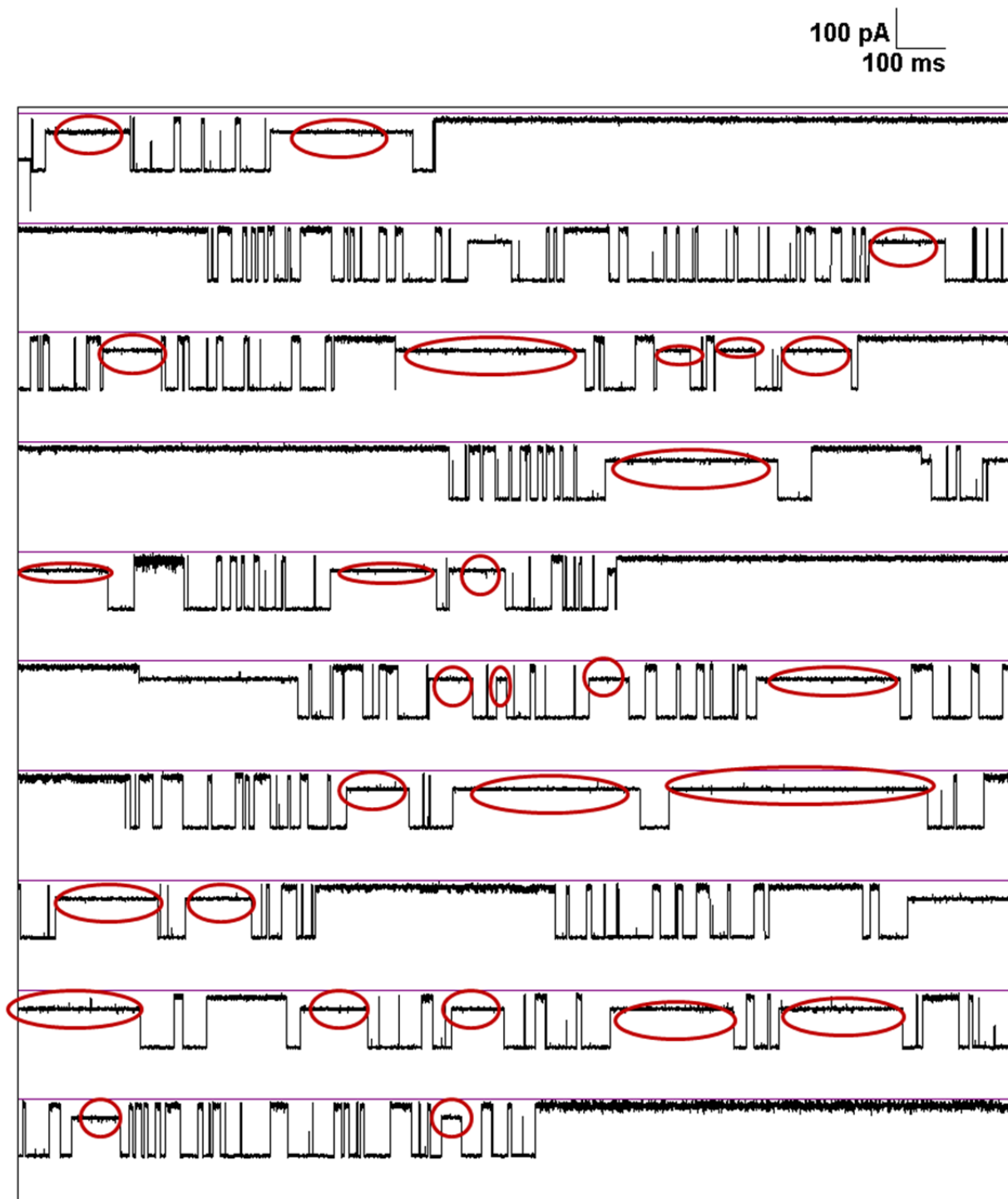


Figure S4. *i-t* traces for a dumbbell sequence at 100 mV (*trans* vs. *cis*). The sequence of the dumbbell is: 5'-GAACG GTTA CGTTC GAACG GTTA CGTTC-3'. Greater than 95% of the events showed mid-level blocking currents (30-50 % I_0).

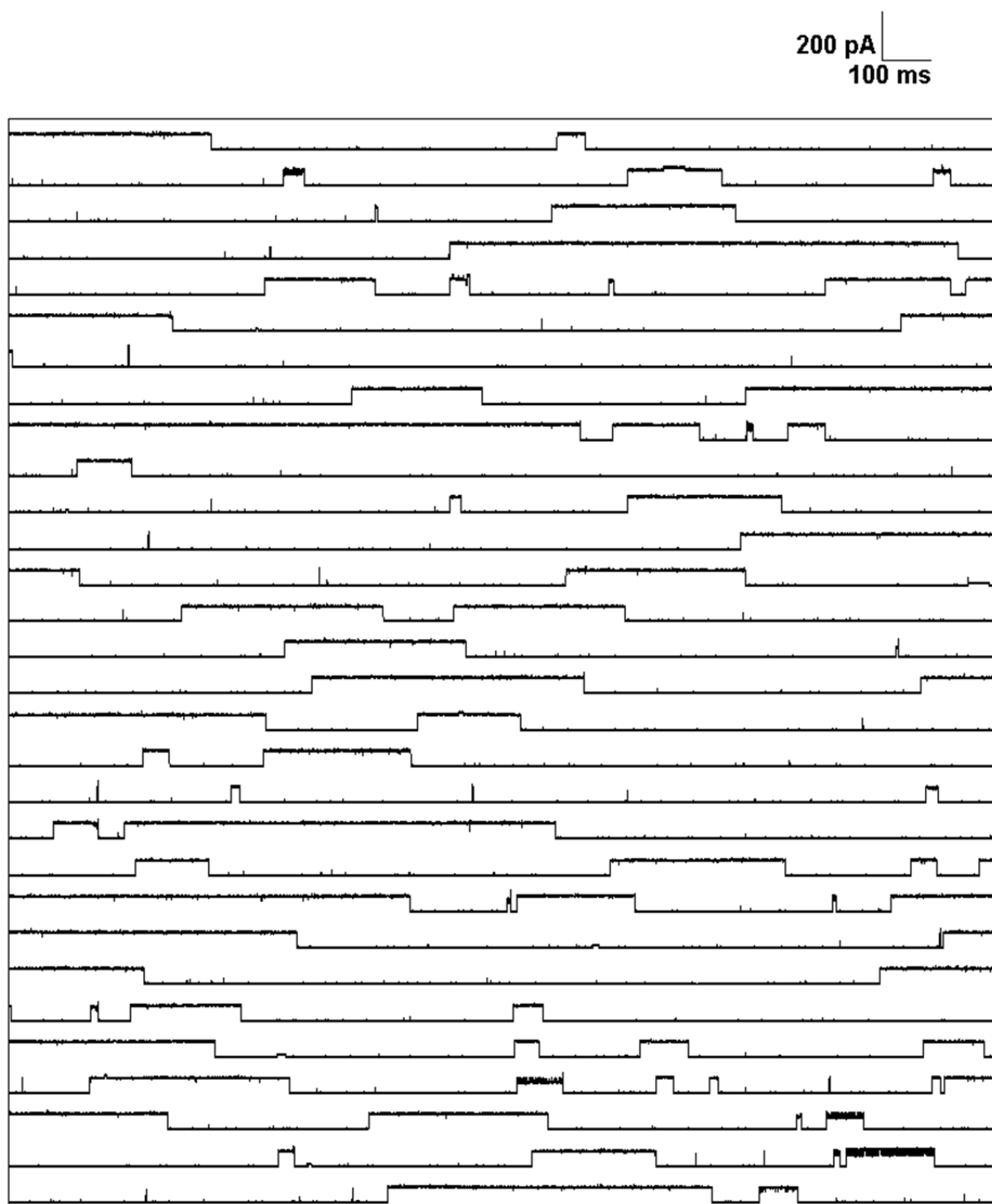
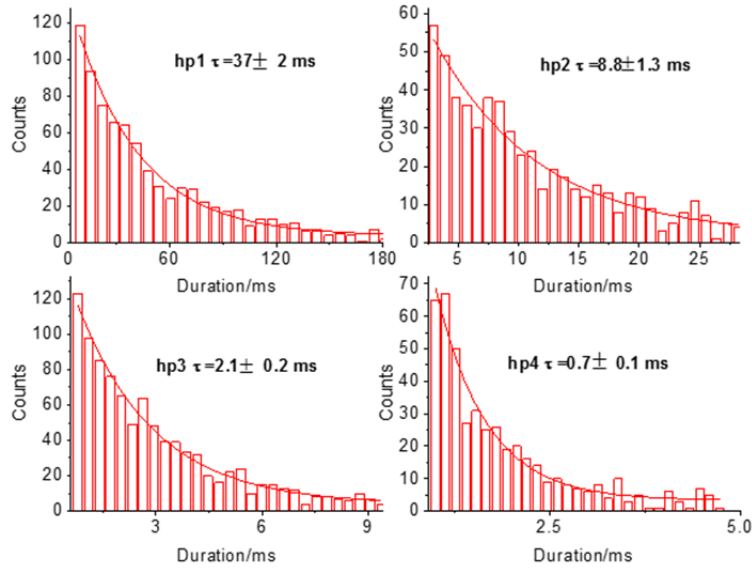


Figure S5. Single exponential decay fitting of data for internal hairpins I-hp12-1, 2, 3, and 4 at 80 mV (A) and at 100 mV (B).

A:



B:

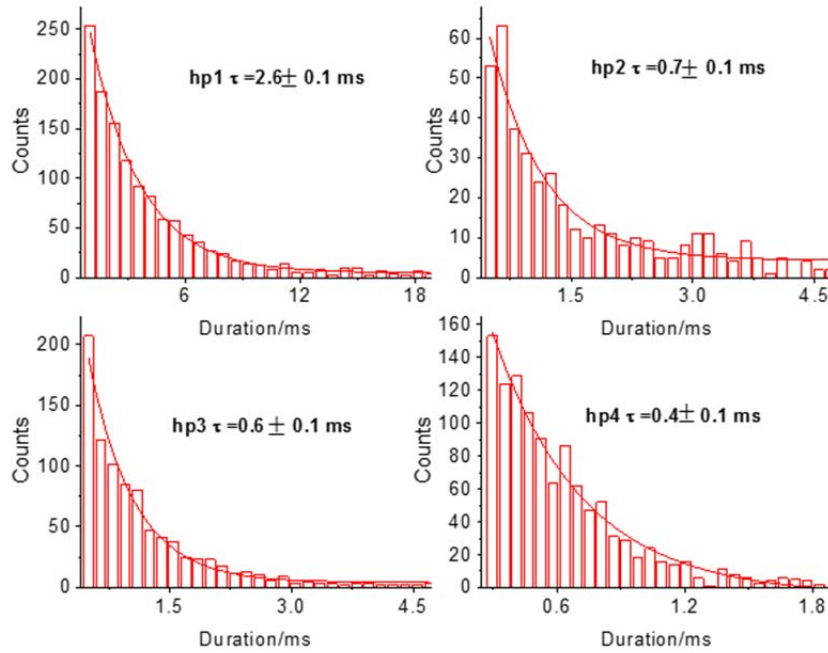


Figure S6. Voltage-dependent study of internal hairpins and fishhook hairpins. The unzipping times of internal hairpins show a stronger voltage dependence than fishhook hairpins. In the current study, we did not try to determine the physical bases for this observation

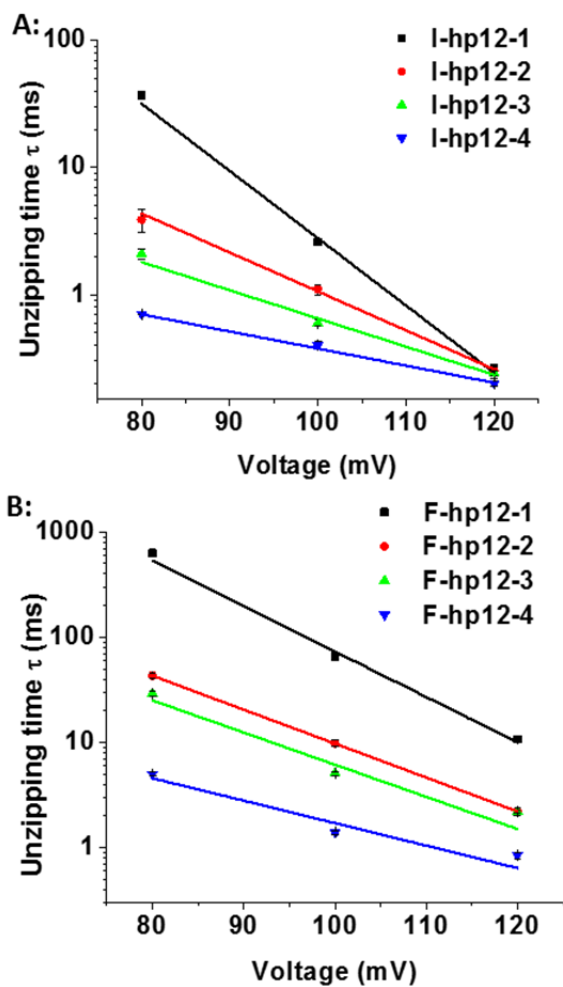


Figure S7. Single exponential decay fitting of unzipping time distribution for hp6, hp9, hp12, and hp15 at 80 mV (A) and 100 mV (B). The sequences of these internal hairpins are provided in Figure 4A. Because hp6 was not very stable and translocated through the nanopore channel too fast, I_A and I_B could not be differentiated in the $i-t$ traces. The unzipping time distribution for hp6 is more like Gaussian distribution, however, it is still fitted by exponential decay to be consistent with all the other fittings.

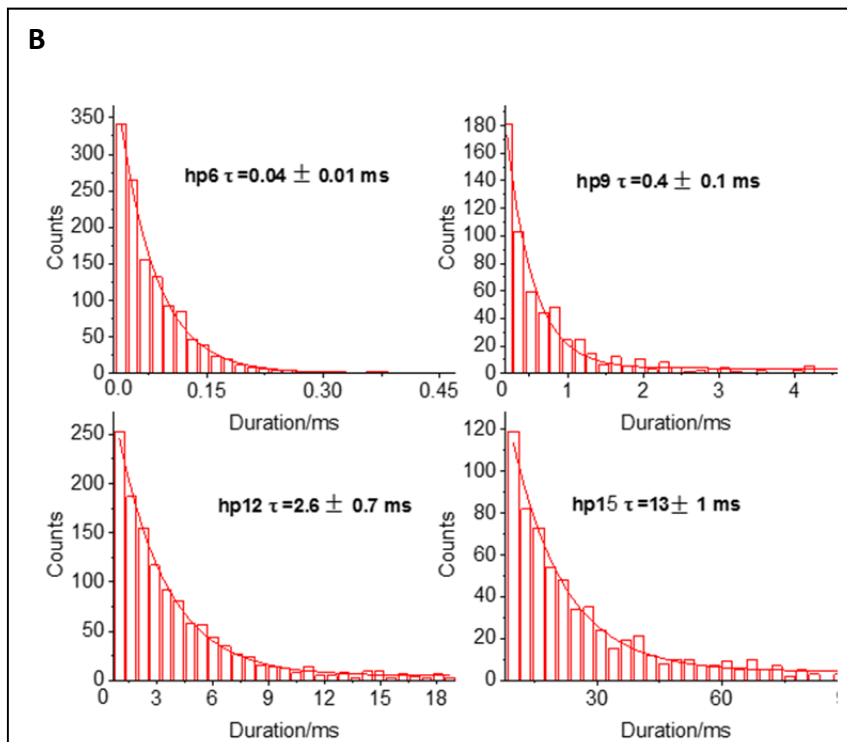
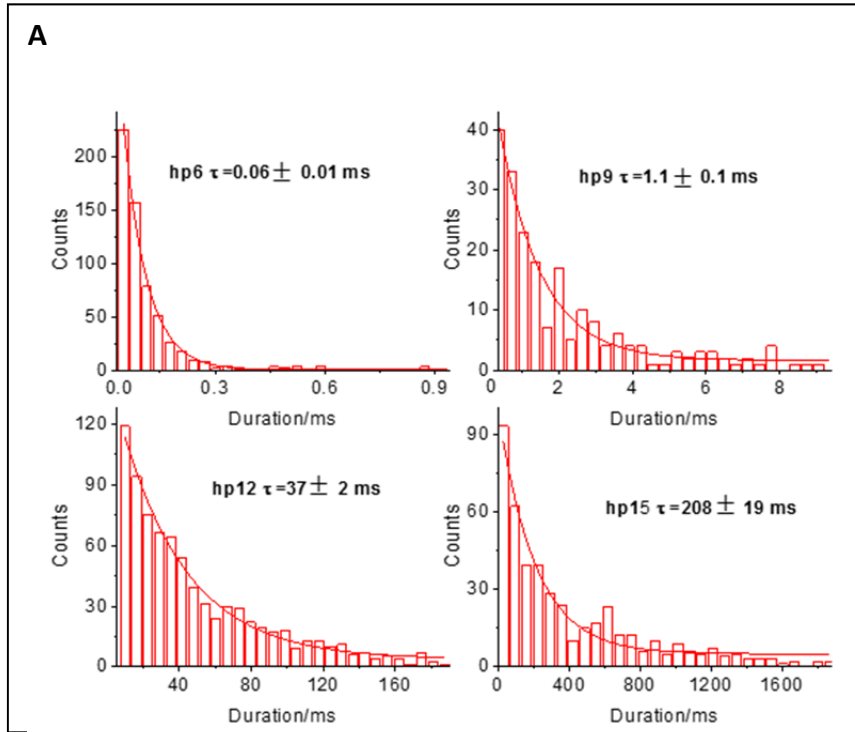


Figure S8. Single exponential decay fitting of data for fishhook F-hp12-1, F-hp12-2, F-hp12-3, and F-hp12-4 at 80 mV (A) and 100 mV (B).

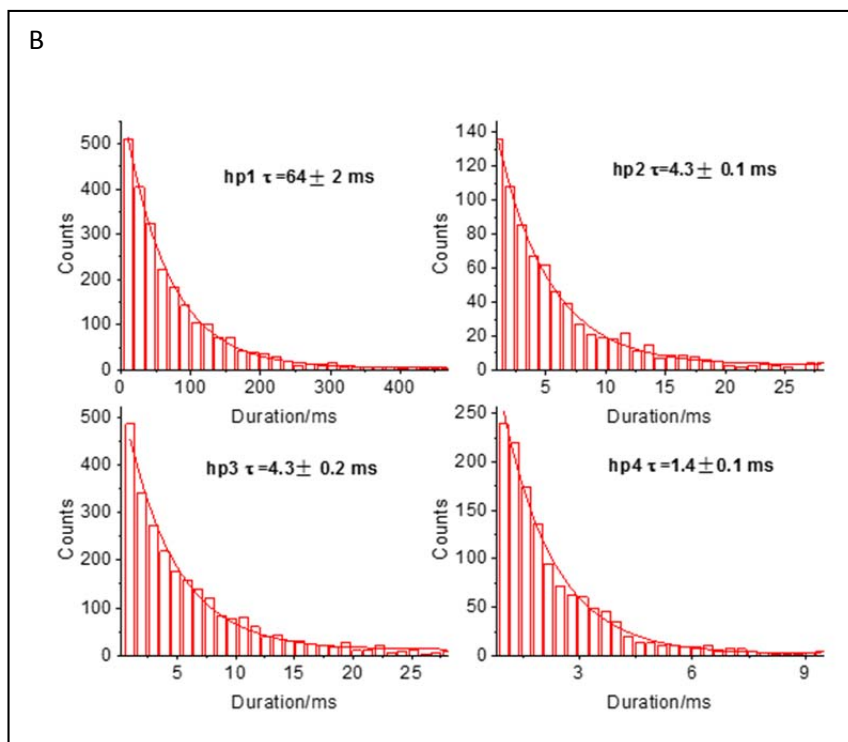
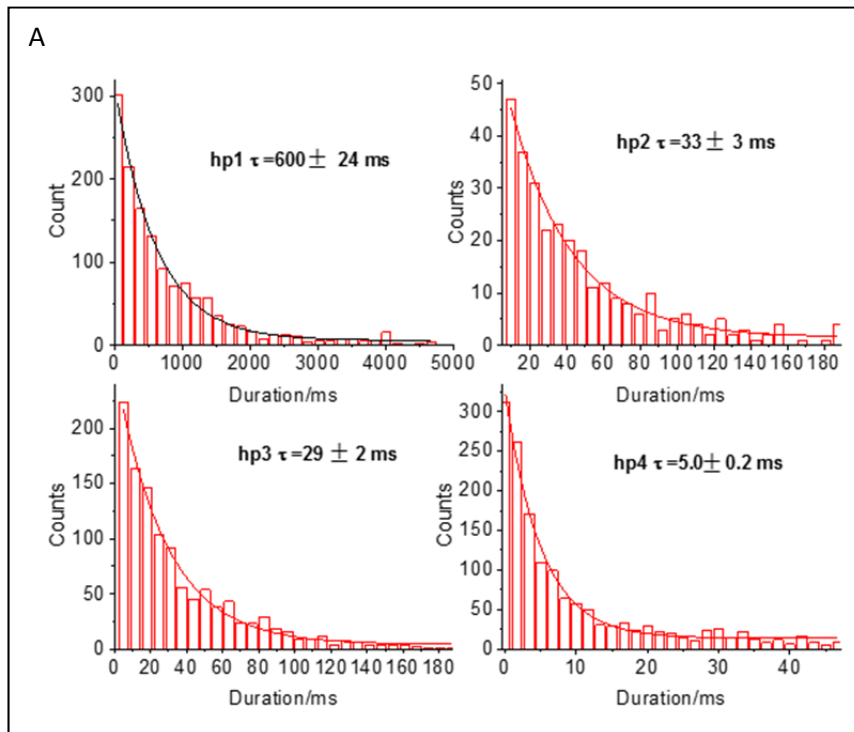


Figure S9. Urea denaturation study of internal hairpins for I-hp12-1, I-hp12-2, I-hp12-3, I-hp12-4 at 100 mV (*trans* vs. *cis*). The 2 M urea was used in this study. All four internal hairpins translocated with similar times (~ 0.7 ms) in the presence of urea, consistent with all four hairpins having the same overall length. This study further supports the observation that the identity of the terminal base pairs is critical in the initiation of the unzipping process.

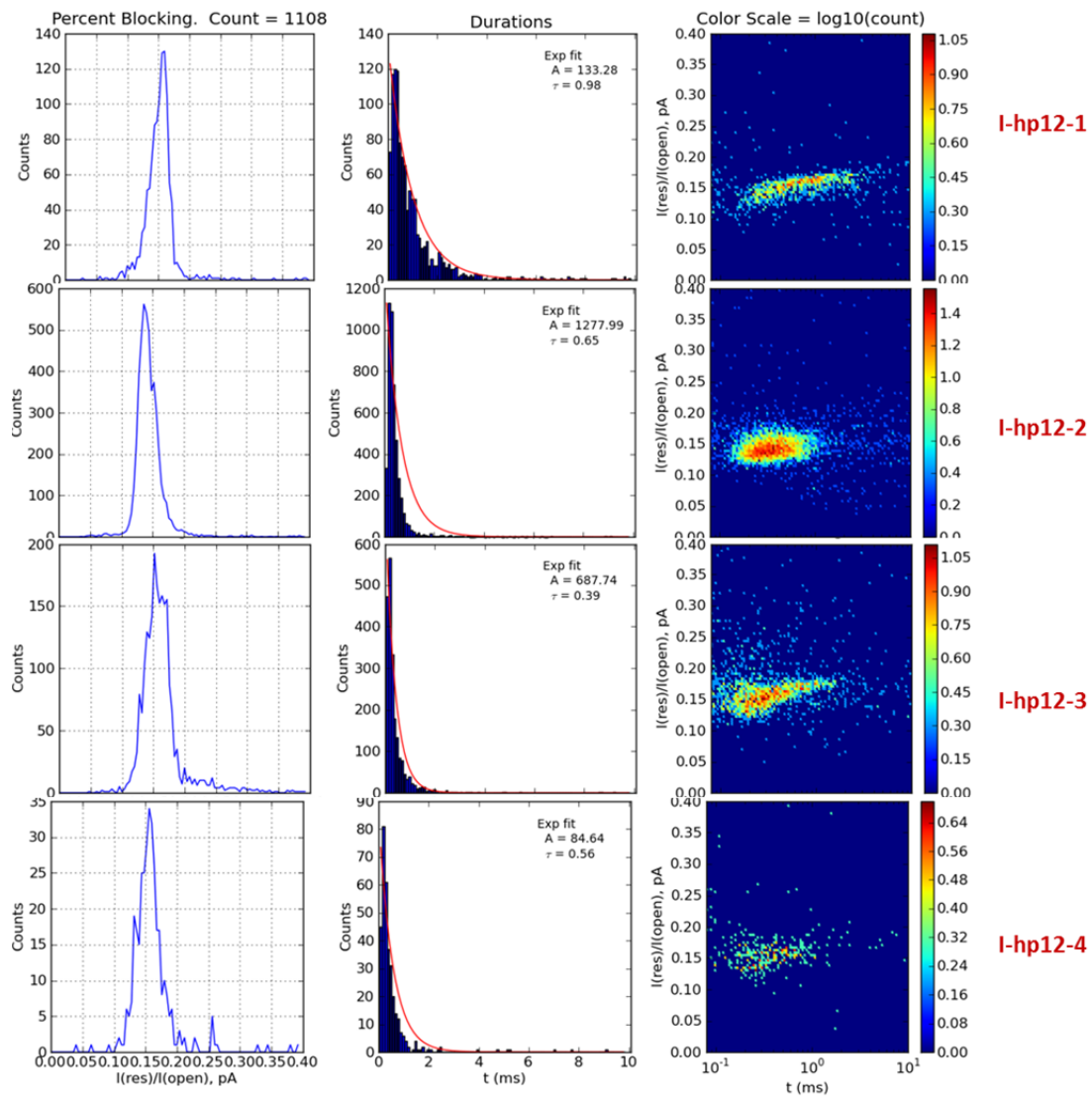


Figure S10. The unzipping time distribution and the 2D plots for internal hairpin I-hp12-1 at 80 mV, 100 mV, and 120 mV. The unzipping times decreased as the voltage was increased. At lower voltage, two stripes can be observed, corresponding to 3' and 5' entry; the two stripes disappeared as the voltage was increased due to the short residence time in the channel.

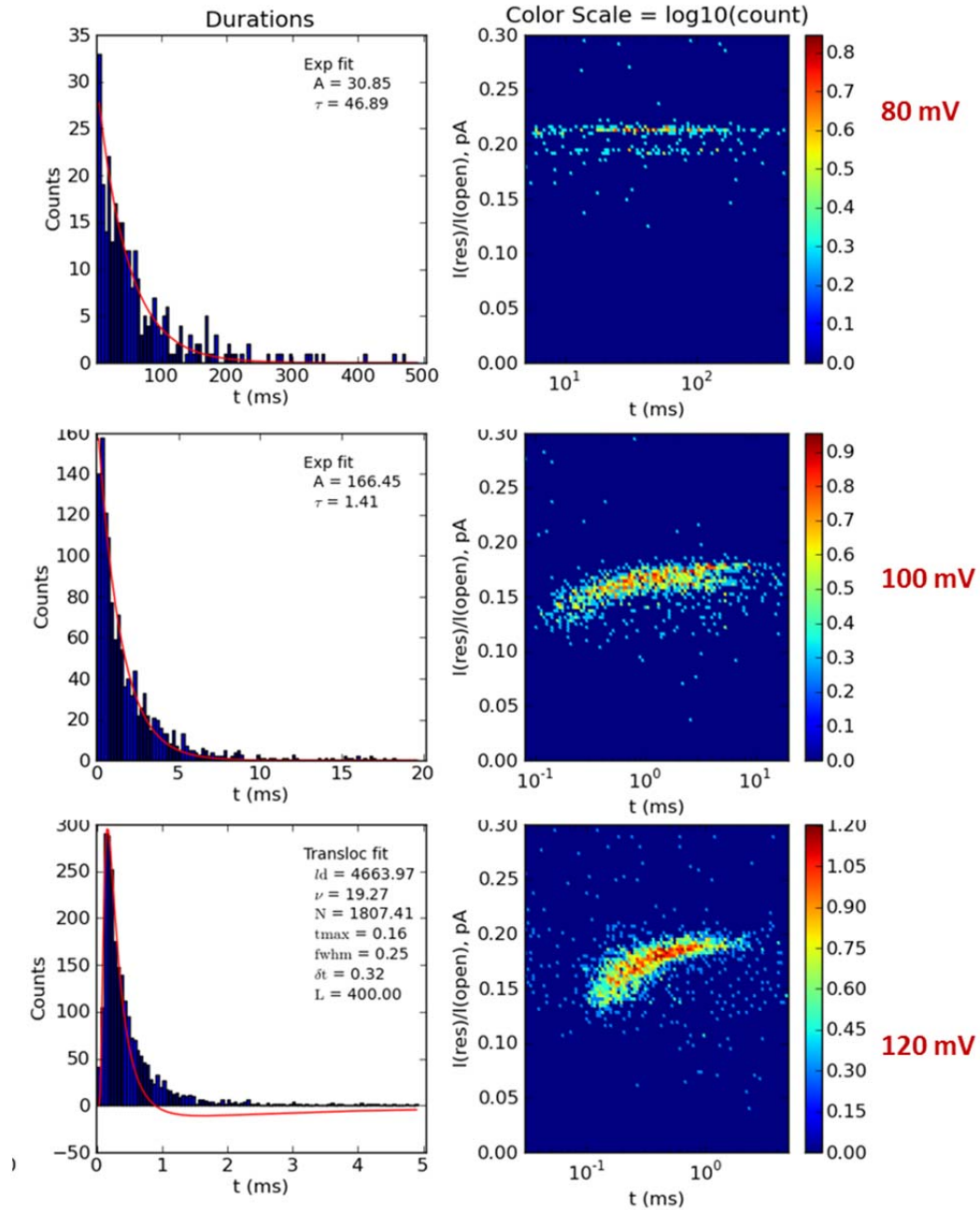
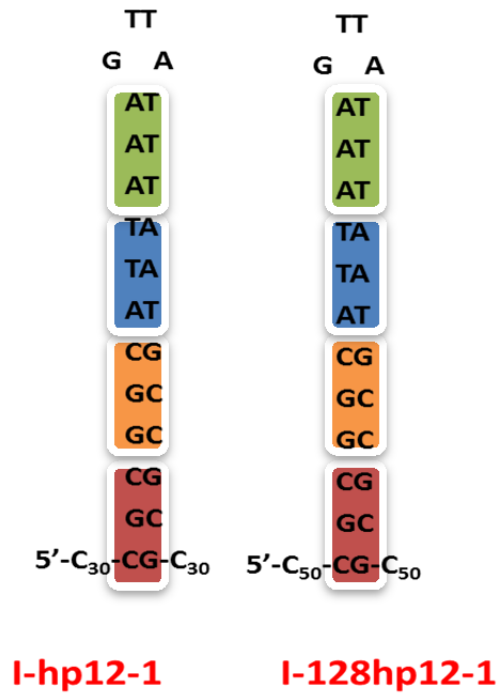


Figure S11. The unzipping of two internal hairpins with different tail lengths at different voltages. To exclude the possibility that the difference between internal hairpins and fishhook hairpins were caused by the length of the tail, another unzipping experiment was conducted with I-hp12-1 (A). The only difference between I-hp12-1 and I-128hp12-1 is the length of tails, in which I-hp12-1 has dC₃₀ tails and I-128hp12-1 has dC₅₀ tails. The similar unzipping times are compared in (B), indicating that it is not the tail length that causes the different behaviors between internal hairpins and fishhook hairpins. This study rules out the possibility that the dC₃₀ tails were insufficiently long to unzip the internal hairpins.

A:



B:

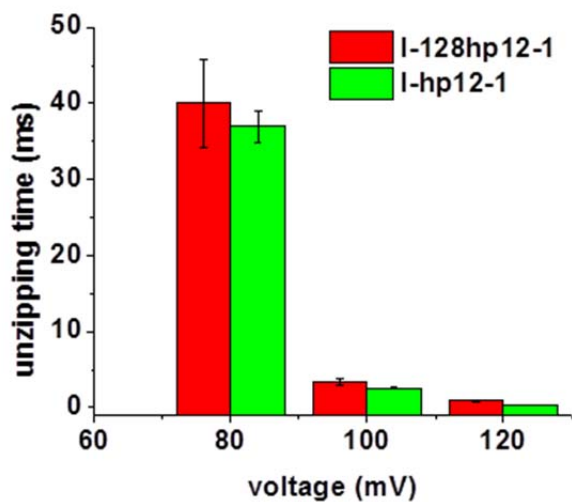


Figure S12. Unzipping directionality of internal hairpins. Two internal hairpins with asymmetric tails were tested in this experiment. One of them has a dC₃₀ tail at the 5' end and a dC₁₂ tail at the 3' end that will only allow 5' entry into the α -HL nanopore. The other one has a dC₁₂ tail at 5' end and a dC₃₀ at 3' end that will only allow 3' entry into the α -HL nanopore. In order to tease out the current levels of 3' and 5' entry for internal hairpin unzipping, the hairpin with the dC₃₀ tail at the 5' was first added to the solution and data collected; then the hairpin with the dC₃₀ tail at the 3' end was added to the same solution and data were collected simultaneously with both molecules. The current levels for each entry are shown in this figure.

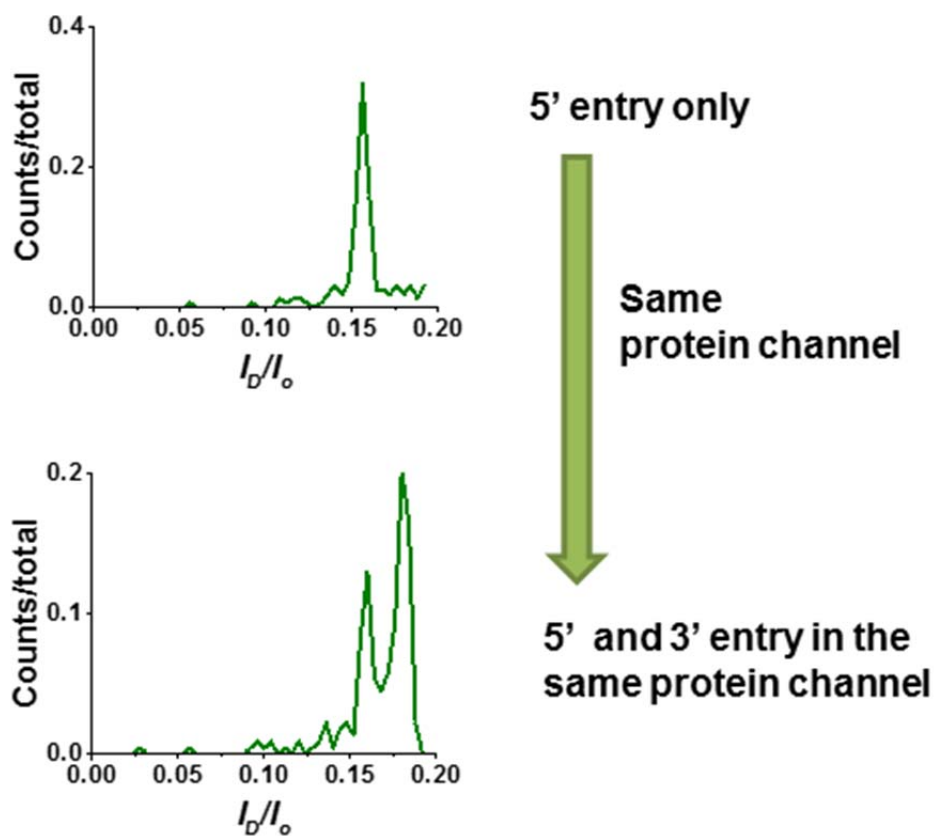


Figure S13. Current time (*i-t*) traces of unzipping F-hp12-1 and I-hp12-1 present simultaneously in the same solution at 100 mV (*trans* vs. *cis*). Data were originally collected with a 100 kHz low pass filter and then filtered to 20 kHz for presentation.

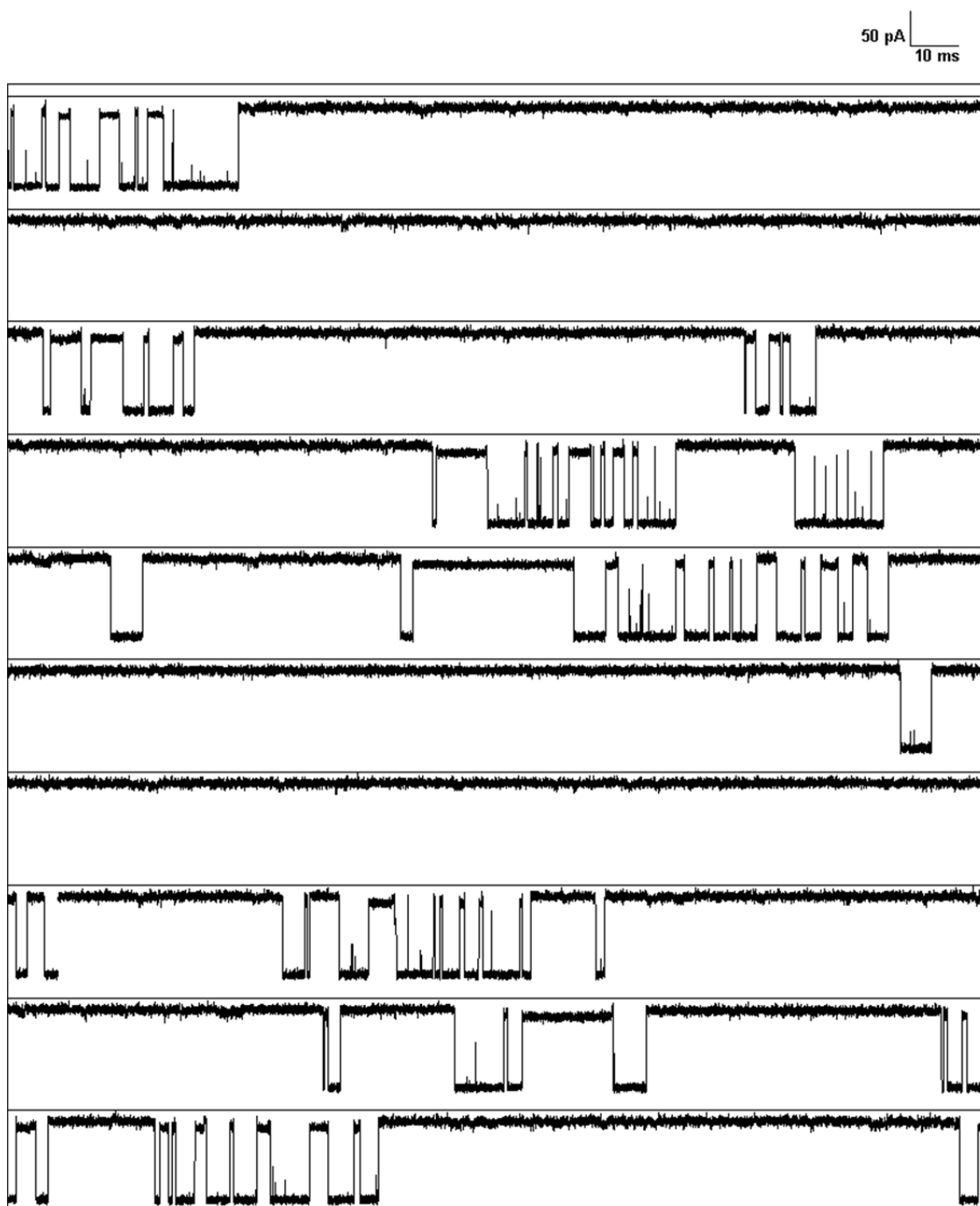


Figure S14. Representative internal hairpin *i-t* traces for I-hp12-1 shown in Figure S9. Data were originally collected with a 100 kHz low pass filter and then filtered to 20 kHz for presentation.

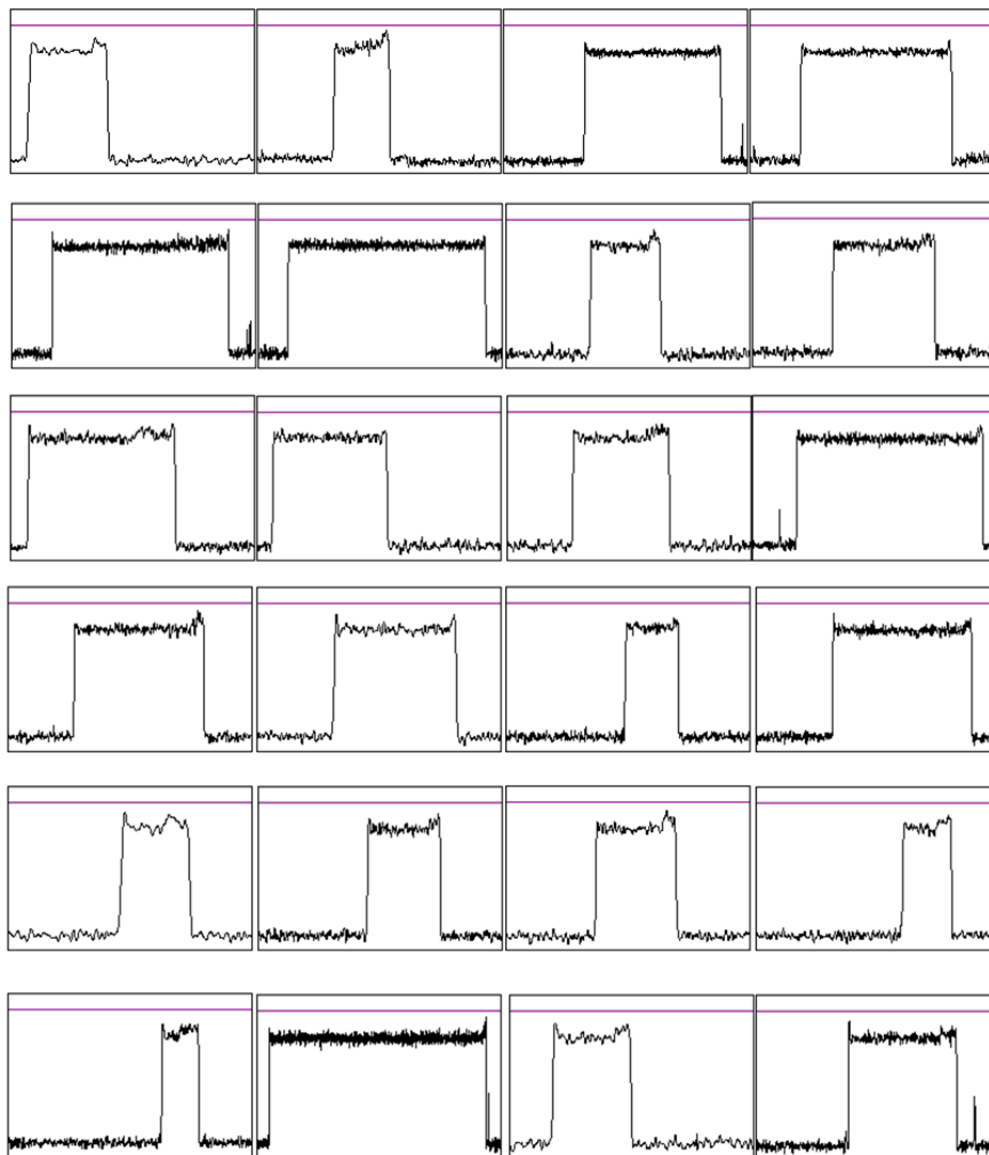


Figure S15. Representative internal hairpin *i-t* traces for the long asymmetric hairpin (Figure 7) at 100 mV (*trans* vs. *cis*). Data were originally collected with a 100 kHz low pass filter and then filtered to 10 kHz for presentation.

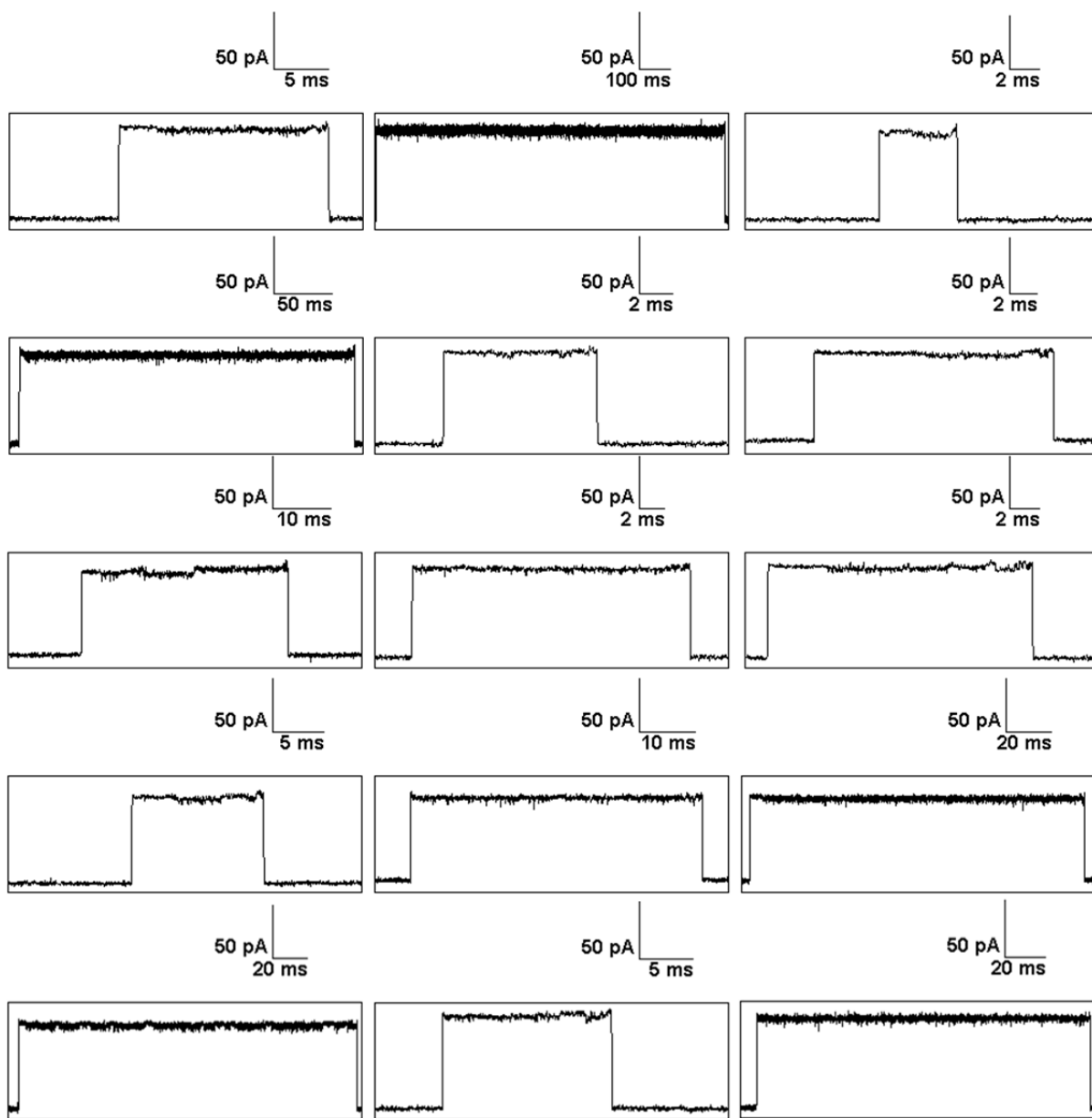


Figure S16. *i-t* traces for I-hp6 at 100 mV (*trans* vs. *cis*). Deep blockage events were less than 1 ms in duration.

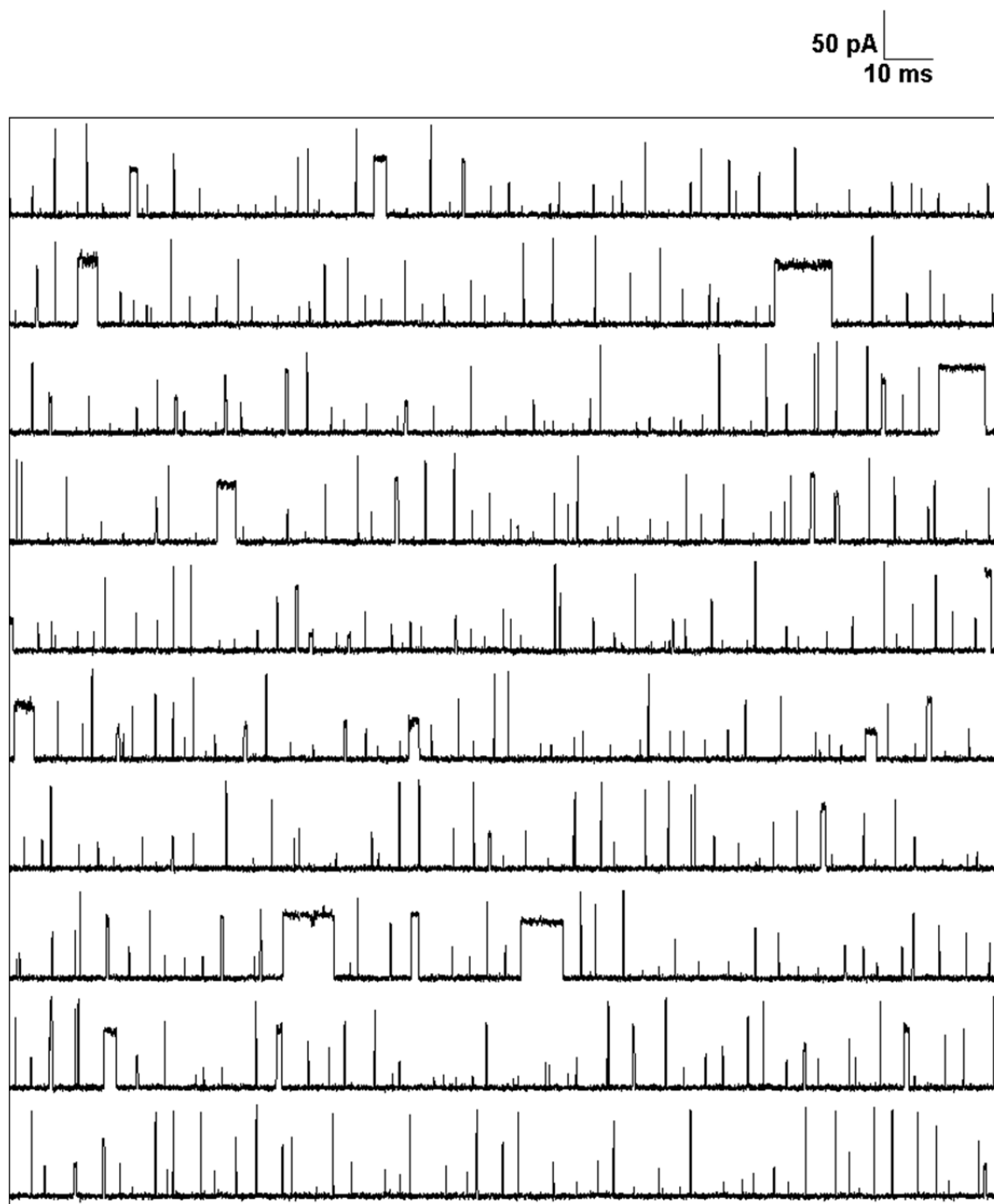


Figure S17. *i-t* traces for I-hp15 at 100 mV (*trans* vs. *cis*). Pulse-like patterns were observed for deep blockage events.

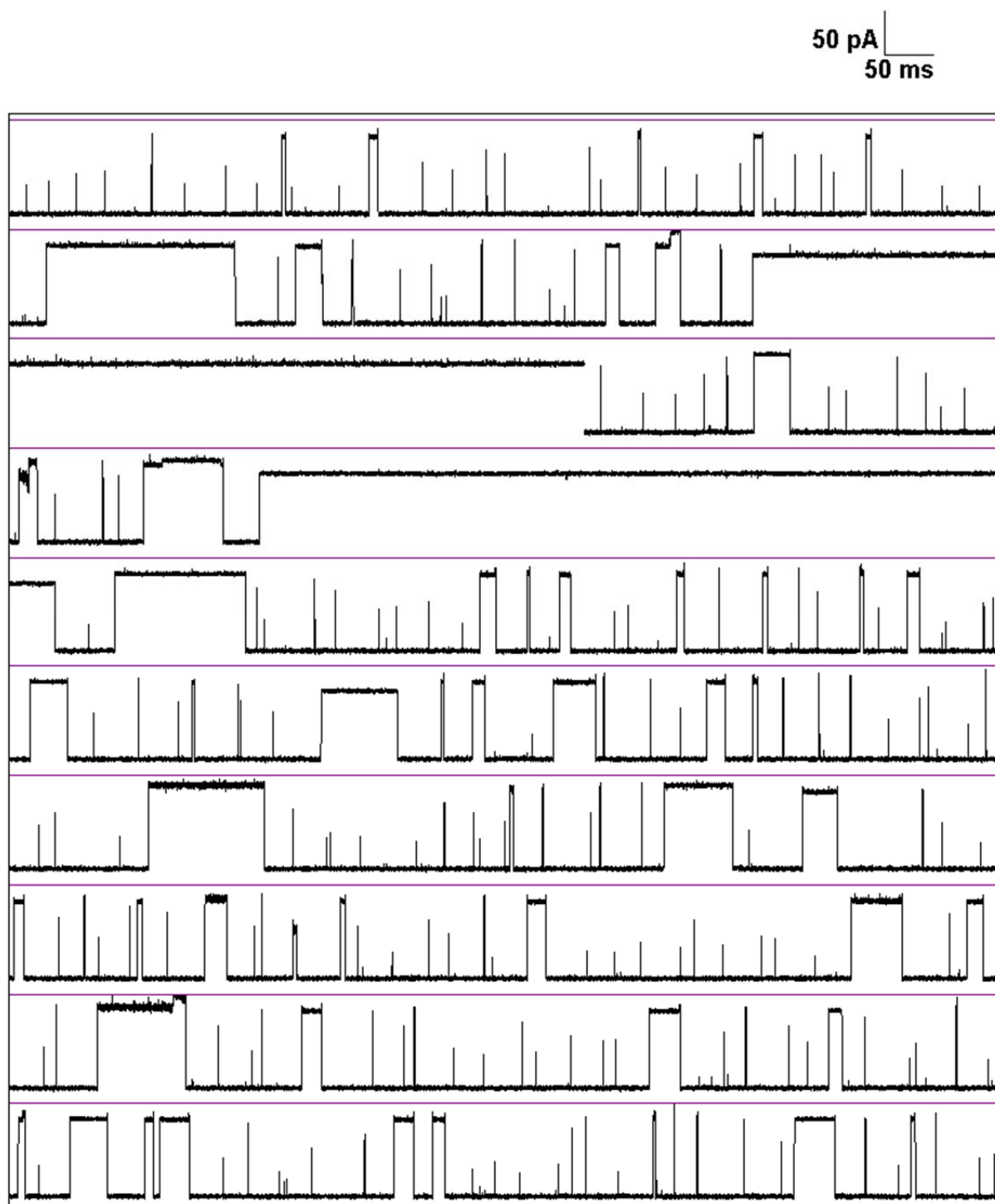


Figure S18. *i-t* traces for internal hairpin with asymmetric tails ($X = 6$) at 100 mV (*trans* vs. *cis*). Only long, deep blockages and loop entry were observed.

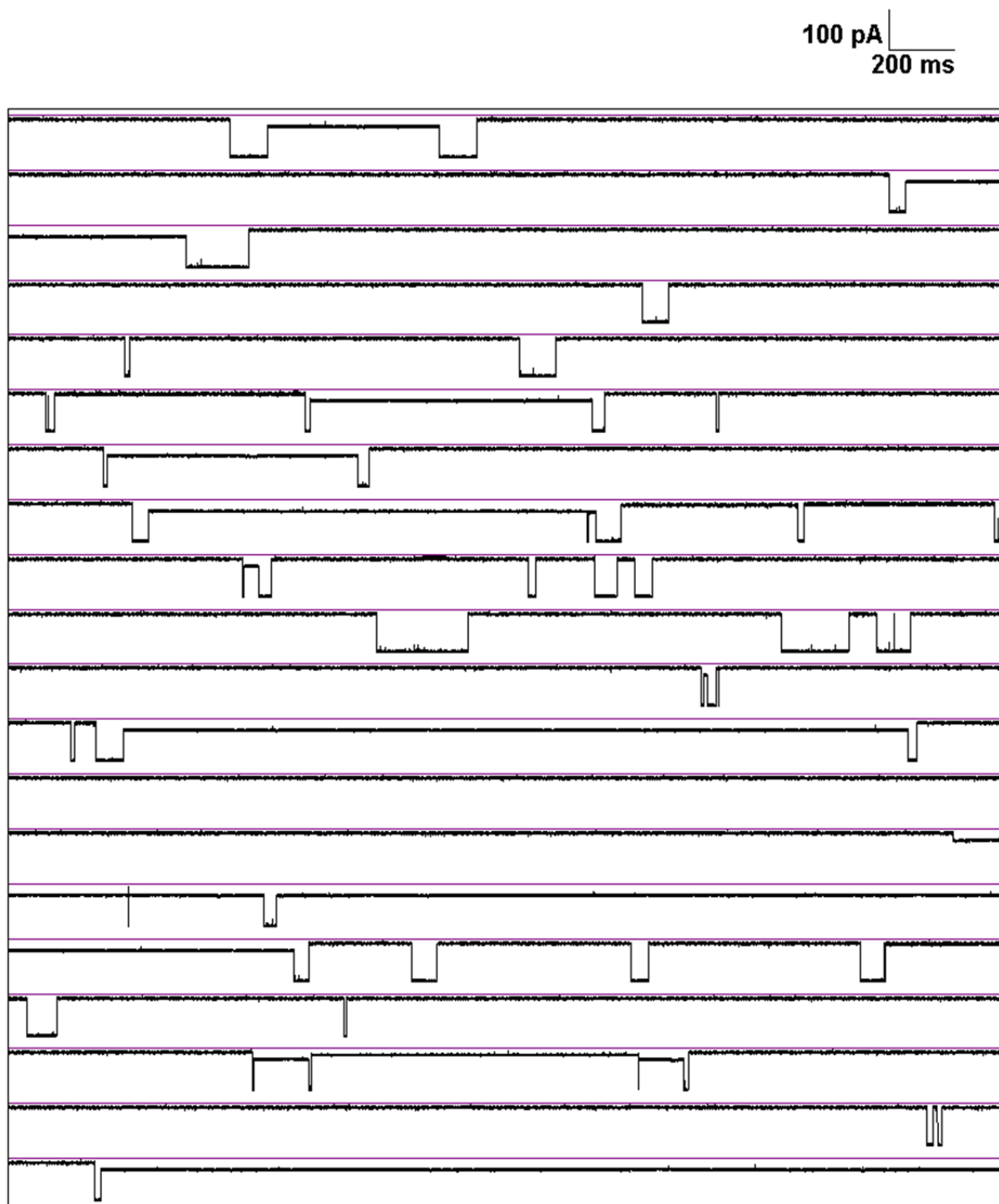


Figure S19. *i-t* traces for internal hairpin with asymmetric tails ($X = 9$) at 100 mV (*trans* vs. *cis*). Besides long, deep blockages and loop entry, short, deep blockages were also observed.

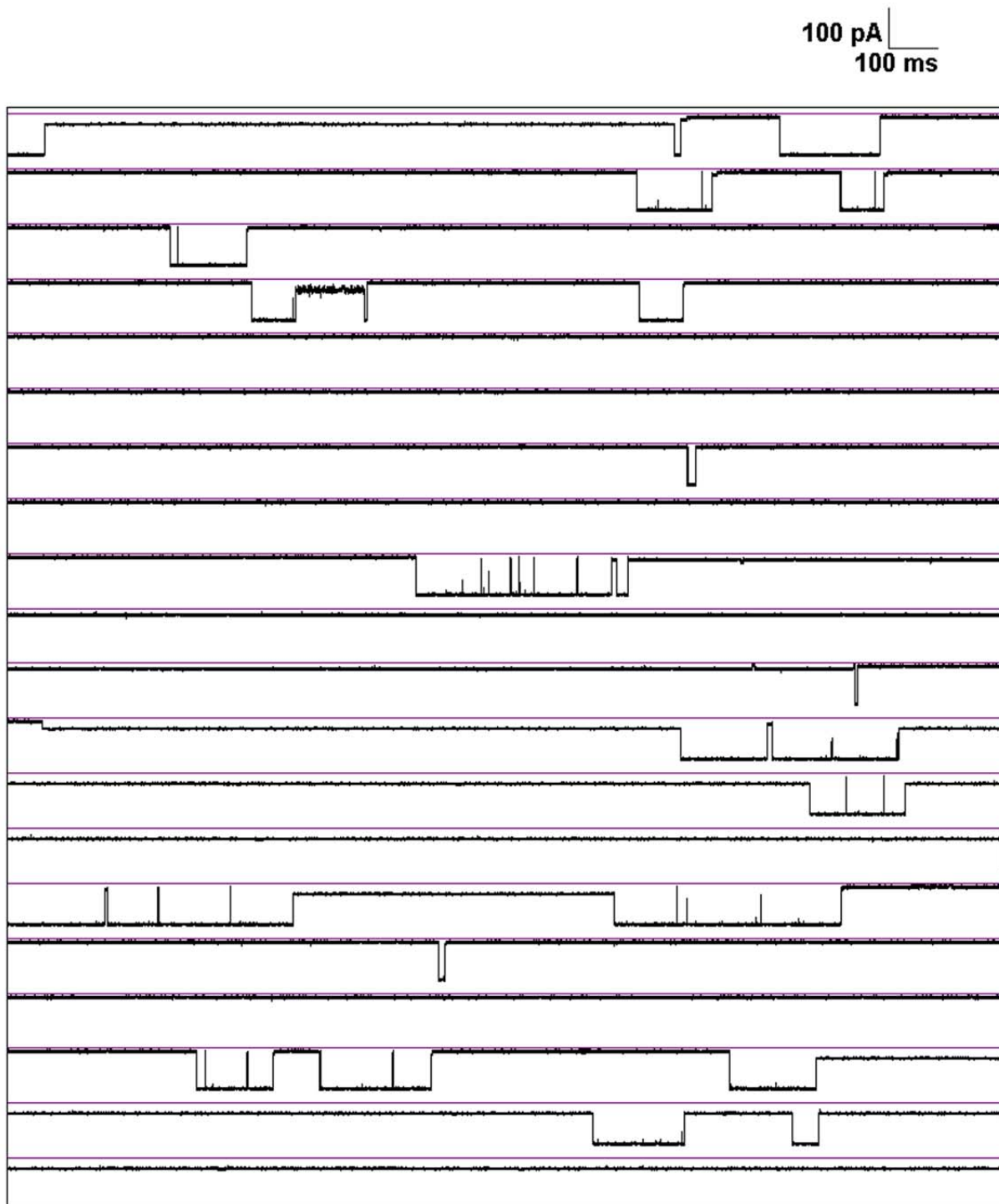


Figure S20. *i-t* traces for internal hairpin with asymmetric tails ($X = 12$) at 100 mV (*trans* vs. *cis*). Fast, deep blockages were observed in addition to loop entry.

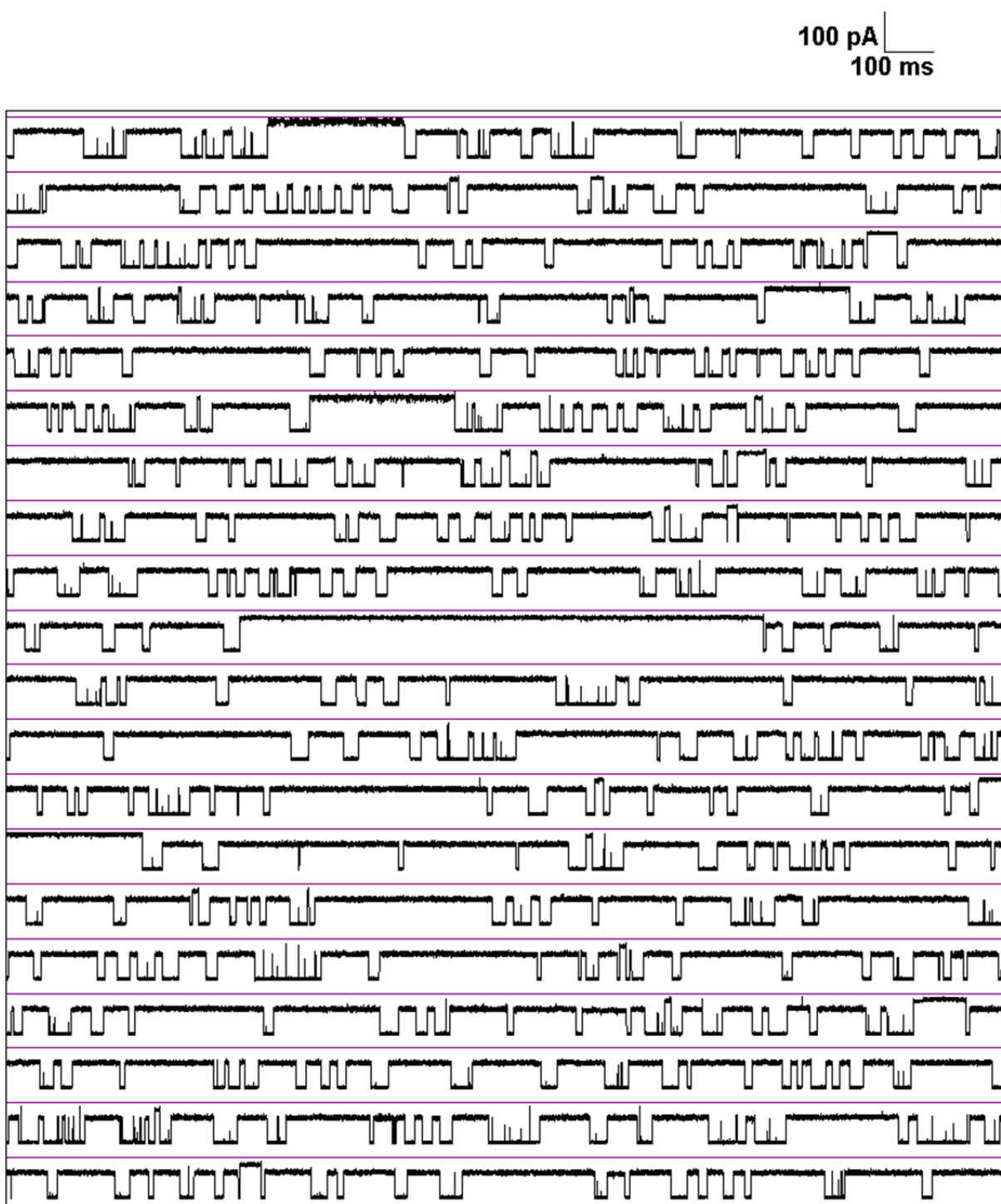


Figure S21. Blocking current of fishhook hairpin 5'C₃₀ CGC GGC ATT AAA GTTA TTT AAT GCC GCG-3' at 100 mV (*trans* vs. *cis*). The 5' entry of fishhook hairpin produced a deep current blockage that is $14 \pm 1\%I_o$. Therefore, 5' entry of the fishhook hairpin is less blocking than 3' entry of fishhook hairpin ($11 \pm 1\%I_o$). And the current level of both 3' and 5' entry of fishhook hairpins are more blocking than the internal hairpin ($18 \pm 1\%I_o$).

